Semiconductor Physics, Quantum Electronics & Optoelectronics. 2002. V. 5, N 4. P. 434-441.

PACS: 42.40.-i

Investigation of synthesis peculiarities inherent to computer-generated rainbow holograms of 3D images

V.I. Girnyk[1], S.A. Kostyukevich[2], P.E. Shepeliavyi[2], A.V. Kononov[1], I.S. Borisov[3]

[1]*Optronics Ltd, PO Box 610, 03127 Kyiv, Ukraine, Phone/fax: +38(044) 560 90 00; e-mail: office@optronics.kiev.ua*
[2]*Institute of Semoconductor Physics, NAS of Ukraine, 45 prospect Nauky, 03012 Kyiv, Ukraine*
[3]*Kyiv Taras Shevchenko University, Radiophysical Dept., 5 B. 2 Acad. Glushkov str., 03137 Kyiv, Ukraine*

Abstract. This work deals with Computer-Generated Rainbow Holograms (CGRHs), which can restore the 3D images under white light. They are devoted to include in Diffractive Optically Variable Image Devices (DOVIDs) that are currently widely used for security needs. CGRHs prevent counterfeiting due to the complexity of recreation, on the one hand, and allow the simple identification at the first (visual) level of verification, on the other hand. To record it, the Electron Beam Lithography (EBL) is used. As recently proved, this method is a most promising for multi-level optical-digital security devices using chalcogenide glasses as resists.
The CGRH computation process is conventionally divided by two parts: synthesizing and recording. On the synthesis stage, firstly, the geometrical and optical constants of recording scheme are determined; secondly, the basic parameters accounting for discretization of Interferogram Data (ID) in hologram plane are defined and, finally, the calculation of the ID – the array of Bipolar Intensity (BI) values – is carried out. This calculation is performed separately in each independent horizontal slice of object space and hologram plane. On the recording stage, suitable quantization parameters are chosen and transformation of ID into the multilevel rectangle data appropriate for EBL is accomplished.
The investigations on optimization of synthesis and recording of the multilevel CGRHs of 3D images integrated in Polygrams are presented here. So the rules for definition of the appropriate discretization parameters were finding out. Advantages of using non-linear quantization that implies condensing of quantization levels near the BI zero were explored. The random deviation of location and direction of elemental hybrid radiating area was applied. Practical applications of the method developed were made using chalcogenide semiconductors of various As-S-Se compositions.

Keywords: computer-generated rainbow holograms, electron beam lithography, diffractive optically variable image devices, bipolar intensity, discretization, quantization.

Paper received 02.12.02; accepted for publication 17.12.02.

1. Introduction

1.1. Destination of CGRHs

Last time the Optical Security Devices (OSDs), also known as Diffractive Optically Variable Image Devices (DOVIDs) become widespread as a reliable and inexpensive mean to protect valuables, documents and goods against counterfeiting. This branch is rapidly developed now, so the invention and development of a new diffractive and holographical imaging methods aimed to prevent counterfeiting and to reduce the possibilities of imitation becomes more and more necessary. From this viewpoint, the CGRHs attract attention, because it can be easily distinguished among other images on the visual level of identificaton, and, at the same time, it can not be manufactured without the Electron Beam Lithography Printing System (EBLPS) or an alternative printing system with the resolution and speed not too worse, thus providing sufficient reliability. We called as Polygram the OSD, which comprises the CGRH as a part. Polygram is similar to a Combigram™, which was reported by us at "Electronic Imaging – 2000" Symposium [1]. Combigrams™ include two different parts: optical recording with a laser, and a digital one made using EBLPS. The latter stage can be realized with a great efficiency when chalcogenide materials are used as recording medium. CGRH can entirely substitute the optical part in Combigram™, because it supposes wider possibilities for object representation and also allows more accurate interaction with the remaining digital part, so we obtain Polygram. The paper [2] was devoted to the first trial fabrication of the separate CGRH using chalcogenide layers.

1.2. Structure of Polygram manufacturing process

Now, the area of a Polygram Elemental Unit (EU) can be divided by the topologies of four different types: ordinary straight diffractive gratings that represent halftone images, curvilinear diffractive gratings representing discs, lenses and other peculiar images, non-diffractive microstructures and eventually the CGRHs topology. Every separate topology take up adjusted region of intended EU. EU separate topology parameters are defined by color of corresponding for EU pixel of image that is respected for separate topology, and separate topology presence in given EU is defined by mask. Thus, the Polygram structure is determined by the amount and type of involved images with related coding images and image masks as well as by EU masks. EU mask for all images, except CGRHs, can be of arbitrary shape. For the CGRHs it must be the rectangle with a strictly confined sizes with a view to considerably simplify manufacturing.

But all of these adjustments are carried out at the second, recording stage of Polygram manufacturing. As regards to CGRHs, the quantization parameters that define the rules for transformation of the ID into multi-level rectangle data are also chosen at this stage. If Polygram contain even one CGRH topology, the first, synthesizing stage is also necessary. First, on the synthesis stage, the basic parameters are defined (Fig. 1a), then geometrical and optical properties of Object Space (OS) represented by surfaces with flat images drawn on it, are determined (Fig. 1b), and finally the calculation of ID – the array of Bipolar Intensity (BI) values – is performed. In the course of this calculation, the fundamental statistic characteristics: minimum, maximum, average and root-mean-square BI values are computed. These values are used then to choose suitable quantization parameters. Let us dwell on physical principles of functioning CGRH and on synthesis of methodology details.

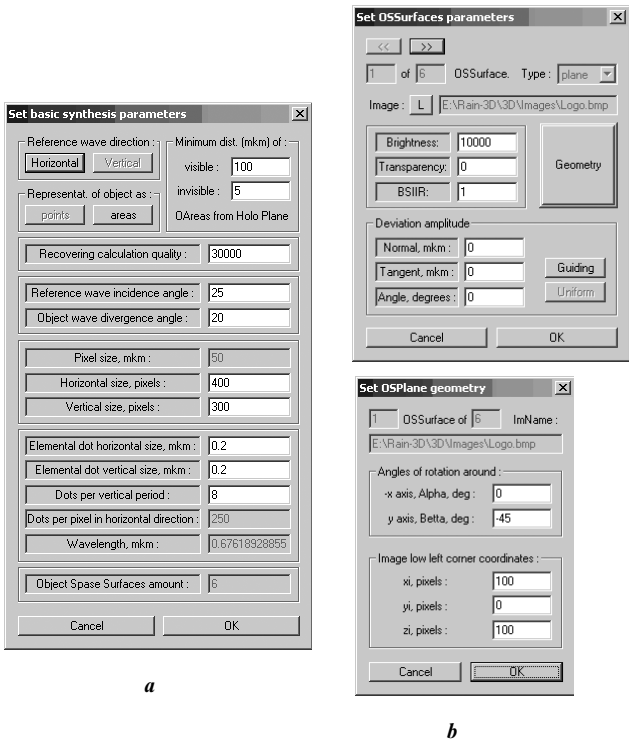

Fig. 1. Synthesis parameters dialogs appearance. *a* – basic parameters dialog; *b* – OS surfaces parameters and plane geometry

1.3. CGRH synthesis methodology

According to rainbow holography principles the object wave divergence angle in definite direction must be essentially restricted. As a rule, the vertical direction is chosen because of the sight physiology. Truncation of the rainbow hologram vertical parallax is equivalent for the division of OS and hologram plane on Independent Horizontal Slices (IHS).

The object elements that get into the given IHS form the separate elemental hologram within it. This elemental hologram restores the correspondent IHS. There is not any influence of one IHS on another at the synthesis process as well as at the reconstruction. The interference fringe (ID) calculation is implemented separately in each IHS only within it. Proceed to the methods of this calculation.

Optical recording allows registering space distribution of the only characteristic: total intensity of all interacting waves (object $\overline{A}$ and reference $\overline{R}$) interference result:

$$I(x,y) = \left|\overline{A}+\overline{R}\right|^2 = \left(\overline{A}+\overline{R}\right)\left(\overline{A}^*+\overline{R}^*\right) =$$
$$= \overline{R}\overline{R}^* + \overline{A}\overline{A}^* + \overline{A}^*\overline{R} + \overline{A}\overline{R}^*. \qquad (1)$$

It is this characteristic that is chosen to be registered in [3-5]. But digital recording supposes richer opportunities as compared with the optical one and allows to register any member of the right part in the expression (1) or their superposition. We chose, as supposed in [6], the Bipolar Intensity (BI):

$$bI = \overline{A}^*\overline{R} + \overline{A}\overline{R}^* = 2\,\mathrm{Re}\left\{\overline{A}\overline{R}^*\right\}, \qquad (2)$$

because it does not comprise neither autocorellation nor constant members, and at the same time is real. The real value registration, unlike the registration of the complex value, sets less rough requirements for the Printing System resolution.

Every IHS is represented as a plane in which the ID calculation is carried out. Object wave is a superposition of spherical waves radiated by every object element. Object can be represented as aggregation of the Self-Radiating Points (SRPs) or as a set of Elemental Hybrid Self-Radiating Areas (EHSRAs). Radiated by SRP wave is described by the following expression:

$$\overline{A_p} = \frac{\sqrt{B}}{r}\exp\left\{j\left(\vec{k}\cdot\vec{r} - \omega t + \varphi\right)\right\}, \quad (3)$$

where B is a brightness of a SRP, $\vec{r}$ is a vector drawn from SRP to the given Vertical Strip (VS) of IHS, j is a complex basis imaging vector, $\vec{k}$ is a wave vector ($k = 2\pi/\lambda$, λ is a wavelength), ω – angular frequency, t – time, φ – initial phase.

For the EHSRA the radiation rule peculiar to the majority of natural sources is taken into account. According with this rule, the light flux radiated by the single area with the normal $\vec{n}$ into arbitrary direction $\vec{r}$ is given by the expression:

$$S = S_0 \cos\angle(\vec{n},\vec{r}) = S_0\frac{\vec{n}\cdot\vec{r}}{nr}, \quad (4)$$

where S_0 is a light flux radiated into normal direction. So, the wave radiated by the EHSRA looks as:

$$\overline{A_a} = \sqrt{\frac{B(\vec{n}\cdot\vec{r})}{r^3}}\exp\left\{j\left(\vec{k}\cdot\vec{r} - \omega t + \varphi\right)\right\}, \quad (5)$$

where n is a single normal to EHSRA.

The wave conjugated to the Reference Wave (RW) looks as:

$$\overline{R}^* = R\cdot\exp\left\{j\left(\eta\cdot(h\cdot x_H + v\cdot y_H + \omega t)\right)\right\}, \quad (6)$$

where $\eta = k\cdot\sin\theta$ is a space frequency of RW phase distribution in the hologram plane (θ – incidence angle of RW), h and v are the coefficients equal respectively 1 and 0 for the Horizontal Direction of RW (HDRW) and 0 and 1 for the vertical one (VDRW). x_H and y_H is a count coordinates in the hologram plane. In accord with (2), it is necessary to sum up contributions of all the SRPs or EHSRAs getting into IHS, for each count $i = 1..N$ ($N = 1$ for HDRW and N is adjusted for VDRW) of period in given Vertical Strip (VS). Contribution of one SRP is obtained by putting (3), (6) into (2):

$$CtbI_i = vis\cdot\frac{\sqrt{B}}{r}\cdot\cos(\pm k\cdot r + \varphi + \eta(h\cdot x_H + v\cdot y_{Hi})), \quad (7)$$

where the coefficient vis is a visibility of the SRP (EHSRA) from the given VS (the coefficient vis takes into account whether SRP (EHSRA) gets into a view region, what side of it is visible from VS, and is it hidden by other EHSRAs or not and how much); the sign "plus" before $k\cdot r$ stays for located under the hologram plane ($z < 0$) EHSRAs, and *vice versa* sign "minus" is selected for the EHSRAs located over the hologram plane ($z > 0$). Similar expression for single EHSRA is obtained by putting (5), (6) into (2):

$$CtbI_i = vis\cdot\sqrt{\frac{B\cdot|(\vec{n}\cdot\vec{r})|}{r^3}}\times$$
$$\times\cos(\pm k\cdot r + \varphi + \eta(h\cdot x_H + v\cdot y_{Hi})). \quad (8)$$

2. Choosing the discretization parameters

Let us define limits of space frequencies of ID alteration in hologram plane distribution. These limits depend on direction (horizontal or vertical) as well as on incidence angle θ of RW and on divergence angle α_{HP} of Object Wave (OW). (Spreading of the OW in horizontal plane (characterized by Horizontal Parallax (HP) angle α) is restricted in limits $-\alpha_{HP} < \alpha < \alpha_{HP}$ in order to exclude high space frequencies that cannot be reproduced by EBLPS). The minimum space period (corresponding to maximum space frequency) for the HDRW is expressed by the following formula:

$$d_{\min} = \frac{\lambda}{\sin\theta + \sin\alpha_{HP}}. \quad (9)$$

For the VDRW interference fringe space period in vertical direction and minimum period in horizontal direction are equal, respectively:

$$d^V = \frac{\lambda}{\sin\theta};\quad d^H_{\min} = \frac{\lambda}{\sin\alpha_{HP}}. \quad (10)$$

According to the discretization Kotelnikov-Shannon theorem for coding the analog signals, the frequency of the sample counts must be at least two times greater then the maximum frequency belonging to the signal. Experimental investigations indicate that the theorem requirements must be fulfilled with the threefold reserve. It means that it must be at least six counts (compare with two counts established by the theorem) per minimum period of diffraction structure.

For the VDRW the elemental dot vertical size and dots per (vertical) period amount are assigned, as shown in Fig. 1a; then d^V is defined and λ is calculated. For the square, elemental dot α_{HP} angle must not exceed angle θ to assure the amount of counts per minimum horizontal period no less then that of vertical period.

As regards to the discretization in object space, it is bound up hard with IHS width. This width has to be sufficient to comprise at least 10–15 vertical periods of each diffractive structure corresponding to (every color channel of) every image.

In the context of the paper we made test recording of five variants of Polygram. Fig. 2 shows the plan of OS surfaces (planes) location and images drawn on it. Basic synthesis parameters are shown in Fig. 1a. Topology location is presented by Fig. 3. In these variants, the quantization parameters were altered, the different approaches for object representation were used, and the noise deviation of location and direction (for EHSRAs) of SRPs or EHSRAs was applied. The results are explained below.

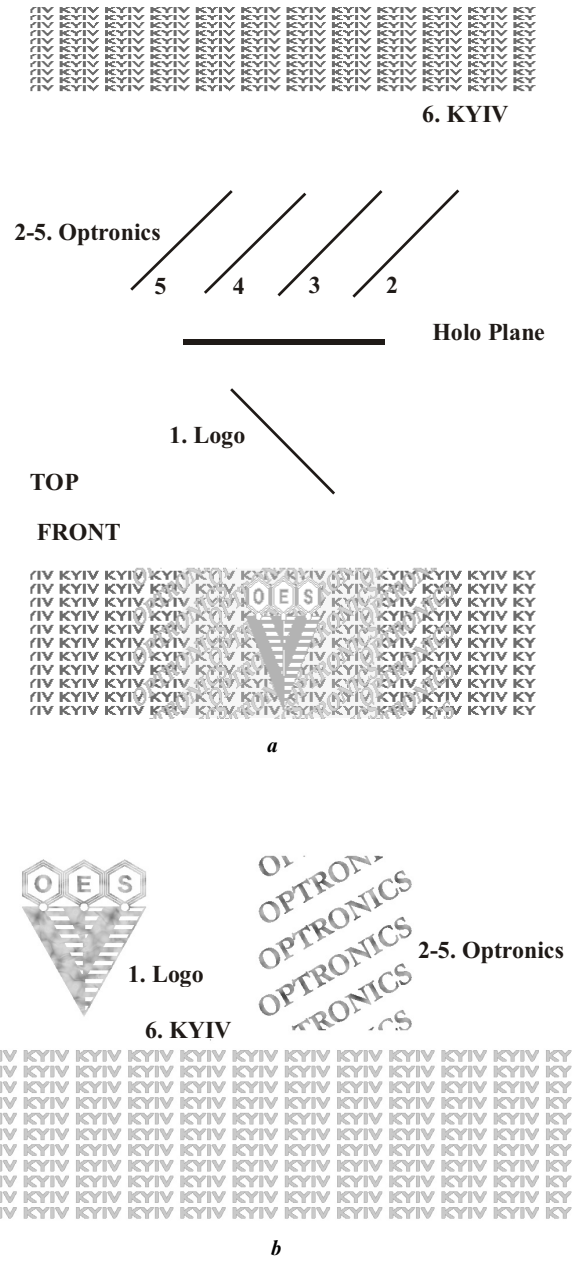

Fig. 2. Setting of Object Space (OS). *a* – 3D scene plan; *b* – images drawn on OS planes

3. Suitable quantization

The available EBLPS provide 16 exposition levels. Together with one more additional level – the absence of exposition – it ensure 17 Quantization Levels (QL). Sure thing, the multiple expositions could provide much more levels, but the time of recording increases pro rata the Quantization Levels Amount (QLA). It would be much better to retain the QLA equal 17 and to improve its using. So, let us mention that the Linear Quantization (LQ) is most fitting for the uniform distribution. However, for the 3D scenes with a complex geometry the BI distribution is close to the gaussian. As to the case, in the distribution centre (BI zero), there is more counts per single BI interval than that of distribution periphery, thus distribution centre requires more detail division. That is why the central quantization intervals have to be more narrow as compared with the peripheral quantization intervals, i.e. the QL condensing near the BI zero is required.

In our work, the following Non-Linear Quantization (NLQ) approach that imply QL condensing is offered. Let us denote the level with the absence of exposition as – 1, the level with the minimum exposition as 0, and so on up to 15-th level with the maximum exposition. Central (7-th) Quantization Interval (QI) binding corresponds to BI zero, the next QI (8-th) binding stand up for Δ from it, the next (9-th) – for $q\Delta$ from 8-th QI binding, 10-th – for $q^2\Delta$ from 9-th, and so on. The quantization is symmetrical relatively to BI zero (Fig. 4). QI borders (quantization thresholds) are defined as:

$$th_n = s_0 + 2\sum_{i=1}^{n} s_i \text{ , where } \frac{s_{i+1}}{s_i} = \sqrt{q} \text{ , } s_0 + s_1 = \Delta \text{ .} \quad (11)$$

To entirely define the quantization rules, two parameters need to be adjusted: TOP that defines the size of BI values clipping interval and q that determines the condensing of QL near BI zero power. Subsidiary parameters can be calculated by the following expressions:

$$L_n = \left(q^n - 1\right)\cdot \Delta \text{ , } th_n = \left(q^n \sqrt{q} - 1\right)\cdot \Delta \text{ ,} \quad (12)$$

where $\Delta = \dfrac{TOP}{q^8 \sqrt{q} - 1}$.

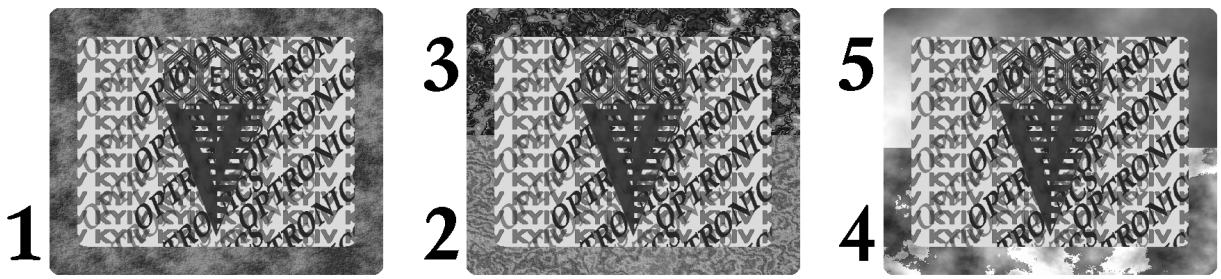

Fig. 3. Topologies of five test Polygrams.

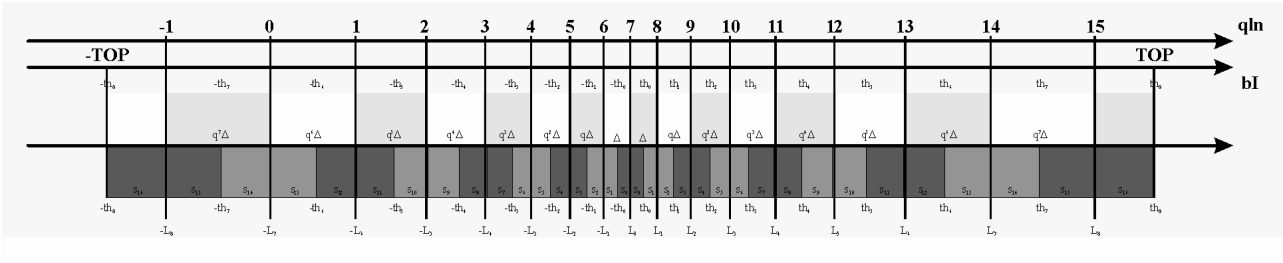

Fig. 4. Choice of QIs borders and bindings (q = 1.21).

Five Polygrams from the test recording mentioned above were recorded with different values of quantization parameters *TOP* and q. The BI distribution is shown in Fig. 5 as well as the distribution of ID on QL. The real histograms are shown overhead (all the BI values getting out from the clipping interval consider equal to its nearest limit) and the coerced to the central peak value BI histograms are given below. The fundamental statistic characteristics: maximum *Max* and root-mean-square σ BI value that is computed during the synthesis stage are cited as well as using values of parameters *TOP* and q. (Minimum is equal to maximum by its absolute value, average is equal to zero). Parameter *TOP* was selected starting from these characteristics. The BI histogram for the third variant coincides with that of the fourth variant, so it is not cited. Fig. 6 shows the micro-fragments of topology for the initial four variants. Comparison of the micro-fragments corresponding to the first and second variants indicates the necessity of the correct choice of BI clipping interval borders (parameter *TOP*): contrast has increased (more QLs is involved) and midtones clearness (central QLs division quality) has also increased for the second variant. The midtones clearness as well as the contrast could be increased also with NLQ application (compare topology of third (LQ) and fourth (NLQ) variants that are shown in Fig. 6: midtones are transmitted more accurately for the NLQ).

4. Random deviation of location and orientation of EHSRA

For the objects placed within the planes that form considerable angles with an x axis (from 20°–30° by their absolute value), it was observed strange behavior, viz.

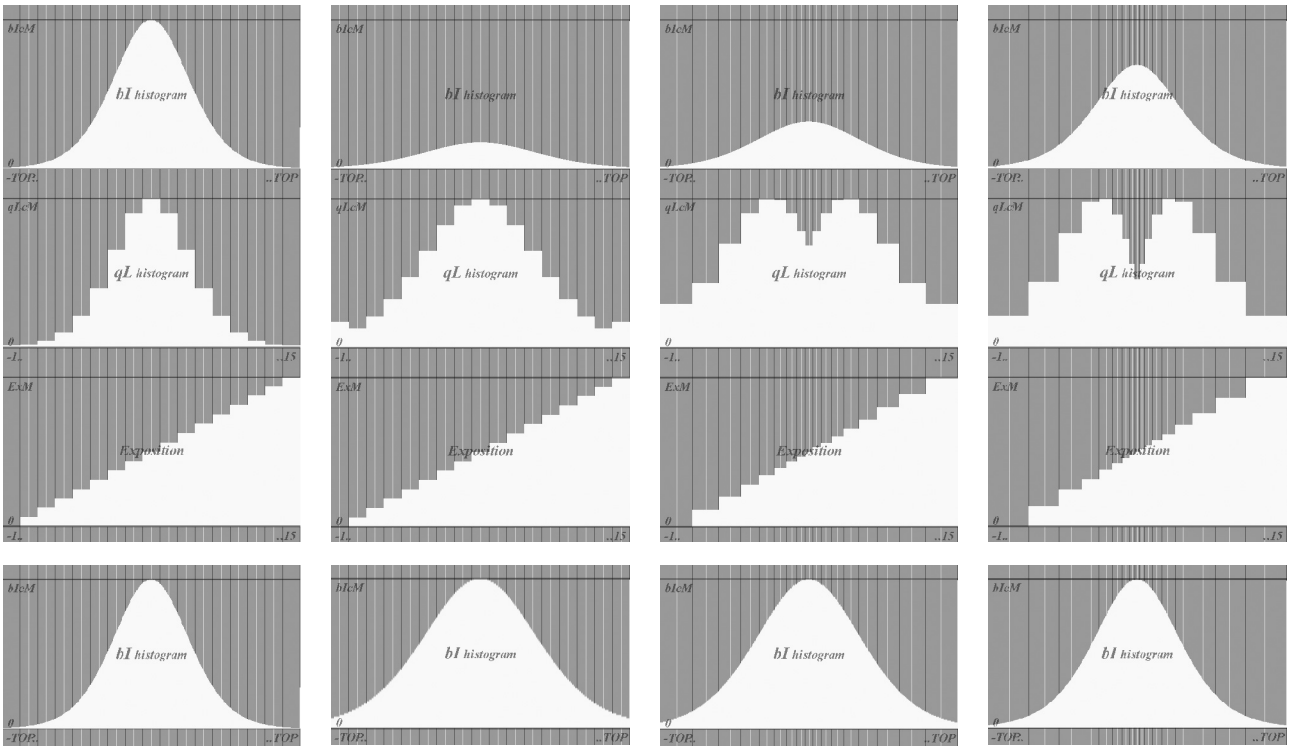

Fig. 5. BI and QL histograms for different values of quantization parameters *TOP* and q. 1st variant: NDevP; *Max* = 5.95; σ = 0.84; *TOP* = 3.0; LQ; 2nd variant: NDevP; *Max* = 5.95; σ = 0.84; *TOP* = 2.0; LQ; 4th variant: DevP; *Max* = 6.44; σ = 0.85; *TOP* = 2.1; q = 1.21; 5th variant: DevA; *Max* = 6.18; σ = 0.67; *TOP* = 2.1; q = 1.33.

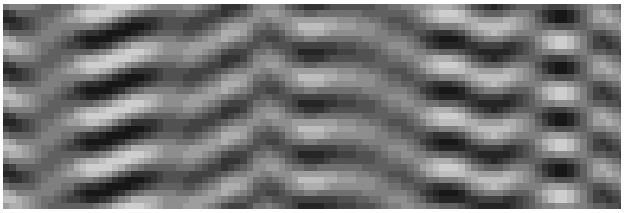

1st variant: NDevP; *Max* = 5.95; σ = 0.84; *TOP* = 3.0; LQ

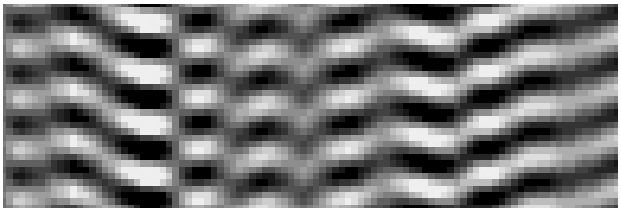

3rd variant: DevP; *Max* = 6.44; σ = 0.85; *TOP* = 2.1; LQ

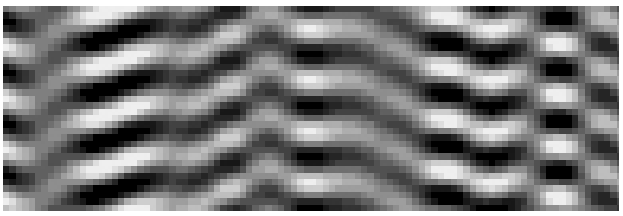

2nd variant: NDevP; *Max* = 5.95; σ = 0.84; *TOP* = 2.0; LQ

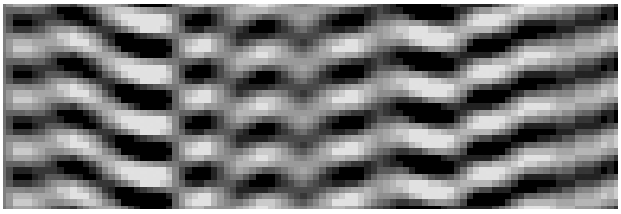

4th variant: DevP; *Max* = 6.44; σ = 0.85; *TOP* = 2.1; q = 1.21

Fig. 6. Micro-fragments of topology for different values of quantization parameters *TOP* and q.

discontinuous alteration of its brightness with horizontal view angle changing. It means that with changing the horizontal view angle, the object flashes at first, then disappears, then flashes over again, and afresh disappears. Such a behavior is explained by the following hypothesis: the flashes and weakenings are the maximums and minimums of interference of a group of the well-ordered coherent light sources – SRPs or EHSRAs. According with this hypothesis, the imposition of some noise on the neatly order in location (and orientation) of the SRPs (EHSRAs) must suppress this effect of the interference nature.

Let us to introduce this noise in such a manner: let the deviation of EHSRA centre from the well-ordered position would be calculated as a sum of the normal and tangential (relatively to well-ordered EHSRA) deviation with the adjusted amplitudes A_n and A_τ, respectively. Let the angle deviation of EHSRA normal from the original well-ordered direction would be calculated with adjusted amplitude B as well. In this case, if the centre coordinates (x, z) and a single normal projections (n_x, n_z) for the well-ordered EHSRA are known, the new coordinates of a randomly deviated centre as well as a new projections of a randomly declined normal could be calculated using the following expressions:

$$\begin{cases} x' = x + A_n n_x \cdot \cos R_1 + A_\tau n_z \cdot \cos R_2 \\ z' = z + A_n n_z \cdot \cos R_1 - A_\tau n_x \cdot \cos R_2 \end{cases} \tag{13}$$

$$\begin{cases} n'_x = \sin(arctg \dfrac{n_x}{n_z} + B \cdot \cos R_3) \\ n'_z = \cos(arctg \dfrac{n_x}{n_z} + B \cdot \cos R_3) \end{cases} \tag{14}$$

where $R_1, R_2, R_3 \in (0, 2\pi)$ are the random phases that are generated independently for each separate EHSRA of an object. Amplitudes A_n, A_τ, B are assigned to each separate object.

For the first and the second variants of test Polygram recording cited above, on the synthesis stage, it was used the presentation of an object as an aggregation of SRPs without adding the noise described above – Non-Deviated Points (NDevP). For the third and the fourth variants the presentation as SRPs with the noise imposition – as Deviated Points (DevP) – was used, and, finally, for the fifth variant the EHSRA with the noise imposition – Deviated Area (DevA) – was used as the elemental one of an object. The results revealed that the parasitic brightness oscillations with the horizontal view angle changing remained for the DevP as well as for the NDevP, and that they disappeared for the NDevA presentation. So, the supposed in this paper original presentation of an object as the EHSRAs aggregation is useful not only because of more natural behavior of an object it provides, but also because this presentation helps to suppress parasitic interference effects.

The practical application of the developed method was made using chalcogenide vitreous semiconductor of As-S-Se composition. To demonstrate possibilities of materials with the mentioned composition, we used a standard system for electron-beam lithography ZBA-21 for recording binary diffraction gratings with spatial frequencies in the range 600...1400 mm^{-1}. As-S-Se layers deposited in vacuum onto optically polished substrates were exposed by an electron beam. After that, these layers were etched using the method described in [10], rinsed in deionized water and dried. Diffraction efficiency of the obtained relief gratings (their typical look see in Fig. 7) was determined as a ratio of light intesity directed into the first order to the intensity of the light beam (λ = 632.8 nm) directed along the normal to the grating plane. The dependencies of diffraction efficiency for layers of three different compositions on doses of electron-bram exposure is shown in Fig. 8. It is seen that the most high values

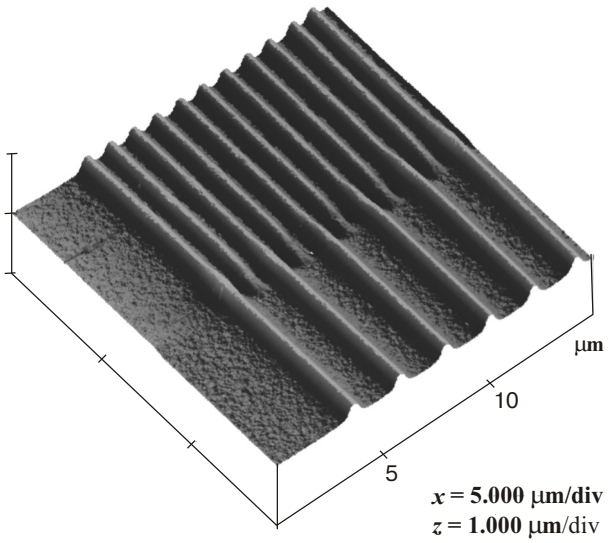

Fig. 7. Typical AFM image of the relief grating made.

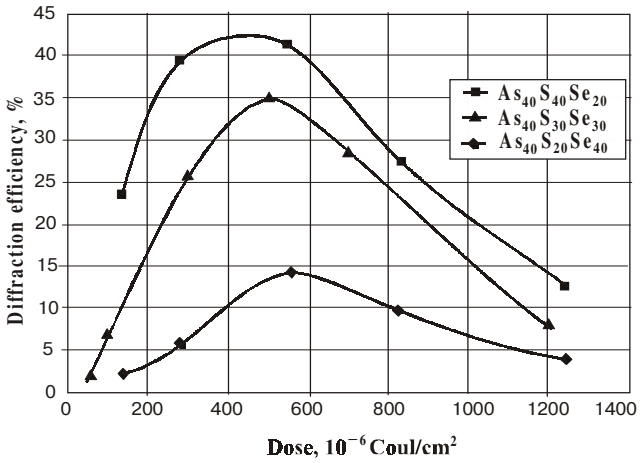

Fig. 8. Dependencies of the diffraction efficiency on a dose of electron-beam exposure for three verious layer compositions.

of diffraction efficiency and exposure sensitivity were reached when using $As_{40}S_{40}Se_{20}$ composition. As to this composition, we studied also the diffraction efficiency dependency on an exposure dose for gratings of various spatial frequencies (Fig. 9).

Results of this investigation show that diffraction efficiency and layer sensitivity at the peak of exposure curves decrease monotonically with increasing the spatial frequency. But in all the investigated ranges of frequencies and doses stay rather high as compared with the other electronic resists. However, the important advantage of these materials is their high sensitivity not only to electron fluxes but to optical recording, too. It enables, using the same medium [11], to realize optico-digital multi-level schemes of manufacturing these safety optical elements.

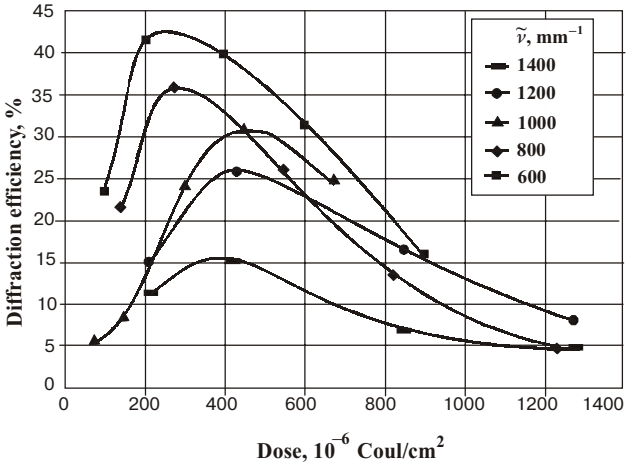

Fig. 9. Dependencies of the diffraction efficiency on an electron-beam exposure dose for gratings of different spatial frequences ($\tilde{\nu}$).

5. Conclusions

In the context of the paper the new type of OSDs developed by authors – the Polygram – and its manufacturing process is described. The article is devoted mainly for the choice of appropriate parameters of synthesis and recording the single CGRH of 3D images that are included in Polygram as a part. So, the experimentally based considerations concerning the discretization parameter choice are cited; the advantages of using non-linear quantization that implies condensing of quantization levels near the BI zero are considered and the original approach for the quantization is proposed and investigated. Authors had come across the problem that object brightness oscillates with horizontal view angle changing. To prevent this parasitic interference effect, the noise imposition on the elemental light sources position was applied. The original presentation of an object as an EHSRAs aggregation came in use for it. The present investigations form the basis for the production of the color, multi-images and combined with another techniques CGRHs that is planned in the nearest future. It will bring up a question how to divide the EU' area among (the different color channels of) the different CGRHs topologies and topologies of the other types.

Acknowledgement

The authors of the paper express their sincere gratitude to co-workers of T. Shevchenko Kyiv National University and the firm "Optronics" for their assistance in making experiments.

References

1. Girnyk V.I., Tverdochleb I.V., Ivanovsky A.A., Combined Optical/Digital Security Devices // *SPIE Proceedings* **3973**, pp.322-327, 2000.
2. Vladimir I. Girnyk, S. Kostyukevych, A. Kononov, I. Borisov, Multilevel computer-generated holograms for reconstructing 3D images in combined optical-digital security devices // *SPIE Proceedings* **4677**, pp.255-266, 2002.
3. T. Hamano, H. Yoshikawa, Image-type CGH by means of e-beam printing // *SPIE Proceedings* **3293**, pp.2-14, 1998.
4. T. Hamano, H. Yoshikawa, Computer-generated holograms with pulse-width modulation for multi-level 3D images // *SPIE Proceedings* **3637**, pp. 244-251, 1999.
5. T. Hamano, M. Kitamura, Computer-generated holograms for reconstructing multi 3D images by space-division recording method // *SPIE Proceedings* **3956**, pp. 23-32, 2000.
6. Mark Lucente, Interactive computation of holograms using a look-up table // *SPIE Proceedings* **1667**, 1992.
7. D. Leseberg, Computer-generated three-dimensional image holograms // *Appl. Opt*. **31**,**2**, pp. 223-229, 1992.
8. A. W. Lohmann, S. Sinzinger, Graphic codes for computer holography // *Appl. Opt.* **34**,**17**, pp. 3172-3178, 1995.
9. H. Yoshikawa, H. Taniguchi, Computer-generated rainbow hologram // *Opt. Rev.* **6**, **2**, pp. 118-123, 1999.
10. E.F. Venger, S.A. Kostyukevich, P.E. Shepeliavyi, Yu.G. Gol'tsov, The way of manufacturing holographic diffraction gratings // Ukrainian Patent No. 36209 with priority from 17 November 1999.
11. S.A. Kostyukevich, N.L. Moskalenko, P.E. Shepeliavyi, V.I. Girnyk, I.V. Tverdokhleb, A.A. Ivanovsky, Using non-organic resist based on As-S-Se chalcogenide glasses for combined optical/digital security devices // Semiconductor Physics, Quantum Electronics and Optoelectronics **4**(1), p. 70-73 (2001).